IOPscience iopscience.iop.org

Home Search Collections Journals About Contact us My IOPscience

ESR in RF-sputtered amorphous GaAs. The As_{Ga}^{+} defect

This article has been downloaded from IOPscience. Please scroll down to see the full text article.

1989 J. Phys.: Condens. Matter 1 9369

(http://iopscience.iop.org/0953-8984/1/47/008)

View the table of contents for this issue, or go to the journal homepage for more

Download details:
IP Address: 171.66.16.96
The article was downloaded on 10/05/2010 at 21:05

Please note that terms and conditions apply.

J. Phys.: Condens. Matter 1 (1989) 9369–9385. Printed in the UK

ESR in RF-sputtered amorphous GaAs. The As^{+}_{Ga} defect

A Deville†, B Gaillard†, K Sedeek‡, H Carchano‡ and K W H Stevens§
† Laboratoire d'Electronique des Milieux Condensés, Université de Provence (CNRS/UA784), Centre de St Jérome, 13397 Marseille Cedex 13, France
‡ Laboratoire de Photoélectricité, Université Aix-Marseille 3, Centre de St Jérome, 13397 Marseille Cedex 13, France
§ Department of Physics, University of Nottingham, Nottingham NG7 2RD, UK

Received 31 January 1989, in final form 19 May 1989

Abstract. We have used ESR at 9.4 GHz and 3.9 K to study the paramagnetic defects in amorphous GaAs prepared by RF sputtering. We show that the complex ESR spectrum originates from three distinct centres. The first one corresponds to the As_{Ga} antisite defect, a well known defect in crystalline GaAs, with its four hyperfine lines and $A \simeq 90$ mT. We use the position and width of the hyperfine structure lines, and a LCAO description to get information on the paramagnetic electron of this defect. The second one, correlated with the first one, is associated with an extra electron from the extra As atom, and with a chemical impurity. The third, a less concentrated one, is probably due to some chemical impurity. We review some concepts used in the field of amorphous solids that are useful for the discussion of our results, and previous ESR results in a-GaAs.

1. Introduction

Crystalline materials present a long-range order associated with a spatial periodicity in the positions of the atoms, leading to characteristic x-ray diffraction patterns, and to an unambiguous determination of the crystalline structures. This periodicity is the starting point for the theoretical study of their electrical properties, and was essential in the establishment of the Bloch theorem and in the band concept. The atomic structure of non-crystalline solids (NCS) is not so unambiguously defined, their physical properties are often found to depend upon the method of fabrication, and the lack of spatial periodicity makes their theoretical study much more difficult than that of their crystalline counterparts. This explains that a somewhat systematic study of NCS started only less than thirty years ago, motivated by some fundamental questions (atomic structure, electronic properties, vibrational properties in the low temperature range, etc.) and technological applications (semi-conductors, metallic alloy glasses, etc.) [1–5]. The study of amorphous GaAs is more recent than that of amorphous Ge or Si (for instance, no results on GaAs are given in [2]), but the motivations are similar. It is well known that the first attempts to dope amorphous Si were unsuccessful, which was then explained by the presence of the so-called 'dangling bonds'; on the contrary, it was possible to dope a-Si deposited by decomposition of silane [6, 7] and hydrogenated a-germanium and silicon deposited by sputtering [8], and this was understood as a saturation of the dangling bonds by hydrogen; this example shows that the presence of defects, even in

very low proportions, may have dramatic effects upon the electronic properties of these materials; it is therefore of interest to detect and characterise such defects. One can think of ESR for this work, when the defects are paramagnetic. In § 2 we recall some concepts and models concerning amorphous materials that are useful for the discussion of our experimental results, and recall some results on amorphous GaAs. Some general comments on the ESR of defects in GaAs, and a summary of the previous results upon the anti-site defect in (mostly crystalline) GaAs and upon other possible paramagnetic centres in amorphous GaAs are given in § 3. We present the sample preparation, the experimental conditions and results in § 4. The experimental spectrum is a superposition of three distinct signals with one of them corresponding to an electron with a strong hyperfine coupling. In § 5 we first show that the problem of determining its A- and g-parameters can be solved exactly. We then use a LCAO description and the positions and widths of the ESR lines to get information about the wavefunction of the paramagnetic electron. We finally discuss the origin of the other signals.

2. Atomic and electronic properties

Diffraction experiments upon NCS only give the radial distribution function (RDF). Even with materials containing only one sort of atoms (e.g. Si, Ge), it is difficult to determine the atomic structure, and the situation is even worse when two sorts of atoms are present (e.g. GaAs). Instead of trying to deduce directly the structure from the experimental data, the approach today is to build atomic models, calculate the diffracted intensity for the model and compare with experiment. If a fit is found, the model is a possible solution [9]. In the discussion of atomic models it is useful to distinguish between *chemical* and *topological* disorder [1]. If, in an initially crystalline material AB, A and B atoms are randomly exchanged, keeping the positions of the sites fixed, the result is a model situation of a NCS with chemical disorder only. If one starts with an A atom, and imagines four B atoms in tetrahedral coordination around it, taking for the bond lengths and angles values approaching the crystalline values, and if the process is repeated for each incorporated atom, one can get a model situation of an amorphous tetrahedral AB compound with topological disorder only. This model is called CRN (continuous random network). Much controversy has existed and several models have been proposed for a-Si and a-Ge (and this is also true for other materials, such as SiO_2 or metallic glasses—for a review see [10]). It is now acknowledged that the position of the first and second peaks of the RDF of Ge and Si is compatible with tetrahedral bonding, and that CRN models, with a small dispersion for bond lengths and angles around their mean values, represent their structure satisfactorily (for instance Polk and Boudreaux [11] found a standard deviation of 0.2% for the length and of 9° around 109.2° for the angle). The first CRN model, developed [12] from the ideas of Zachariasen [13], possesses a great proportion of five-membered rings—about 20%—[14, 15]. Shevchik [14] verified that this model could also explain the x-ray diffraction results for InSb satisfactorily; however the model predicts a high proportion of wrong-bonds (i.e. bonds between like atoms)—about 10%—because of the presence of the five-membered rings. This did not seem realistic. A CRN model with even-membered rings only was then proposed [16], in which it was claimed that this model gave satisfactory agreement with experiment for amorphous Ge, Si and the III–V compounds, and was more realistic. The ratios k_2/k_1, k_3/k_1, k_4/k_1 (where k_i is the position of the ith diffraction peak) deduced from these models were compared [17, 18] with their values in electron diffraction experiments and

it was found that the structure of Si and Ge is better described by a Polk relaxed model, while the Connell–Temkin model is better for the III–V compounds.

The problem of the electronic spectrum of amorphous materials was raised independently by Mott [19] and by Ziman [20] some twenty years ago. Mott observed that the band gap concept had been introduced as a consequence of the spatial periodicity (long-range order), and that ordinary glass, being transparent, should possess a gap. Since the band structure of crystalline Si, Ge and III–V compounds can be explained using the tight-binding approximation, the suggestion is that in these materials the covalent bonding between *nearest neighbours*, responsible for bonding and antibonding states, plays the dominant role. This idea had been developed some time before in another context—that of solid state chemistry. It was then considered [21] that the structure of a (crystalline) solid is essentially determined by two factors: (i) the translational symmetry of the direct lattice, and (ii) the potential within the unit cell. In good conductors the first is the more important, while it is the second in semiconductors. Since diffraction experiments suggest that in IV and III–V NCS the tetrahedral bonding is kept, and since optical absorption and photoemission indicate the existence of a range of energies where the density of states is very weak if not zero (pseudo-gap), it is natural to think that this pseudo-gap reflects mainly the coupling between neighbouring atoms. The theoretical determination of the electronic levels of NCS is a difficult problem (for a review see [22]). This fact has forced the use of simplifying assumptions and the emergence of new ideas. In the case of a-Ge and a-Si it is generally thought now that the experimental facts agree with the ideas of Mott ([23, 24] and [2]) that: (i) the concept of a density of states is still valid in NCS, (ii) when the short range order is the same in the crystalline and in the amorphous materials the gross features of the density of states are the same in both materials, and (iii) because of the disorder, there exists a continuous range of localised states (Anderson localisation). These states are found in the tails of the valence and conduction bands. Cohen, Fritzshe and Ovshinsky supposed at first that both tails overlap (CFO model 1969 [25]). It was then also suggested [23] (Davis–Mott model 1970) and it is now largely accepted that in fact, in amorphous semi-conductors, the bands generally do not overlap. It was shown in [2] that a reasonable value for the tailwidth is a few percent of the bandwidth. The Davis–Mott model also includes the existence of levels within the band gap, resulting from various defects (chemical impurities, dangling bonds, etc.). Information on the electronic levels of a-GaAs was first obtained from reflectivity measurements on films prepared by evaporation [26] (the absorption spectrum has a single, broad and asymmetrical line) and sputtering [27], and from UV photoelectron spectroscopy on sputtered films [15]. Information from flash evaporated films was obtained more recently from reflectivity [28], x-ray photoelectron spectroscopy (XPS) [29, 30], and from a combination of spectrophotometric and photothermal deflection spectroscopy [31]. From these experimental results it was deduced that the chemical order is essentially maintained in a-GaAs (which is not true in GaP or in InP), and that the absorption edge is not sensitive to the presence of an excess of As. The optical gap was found to be of the order of 1.0 eV (after annealing, it increases to 1.15 eV).

3. Previous ESR results on intrinsic defects in crystalline and amorphous GaAs

To date most ESR results in GaAs have been obtained with crystalline samples. However ESR is generally a local probe†, and the local order in amorphous and crystalline GaAs

† Important exceptions are donors in silicon, which possess weakly bound states (i.e. the extra electron has a very large orbit), and conduction electrons in metals.

Table 1. Magnetic characteristics of the natural isotopes in GaAs.

Isotope	Natural abundance (%)	Nuclear spin I	Magnetic moment (unit: nuclear Bohr magneton)
^{69}Ga	40	$\frac{3}{2}$	2.0108
^{71}Ga	60	$\frac{3}{2}$	2.5549
^{75}As	100	$\frac{3}{2}$	1.4349

are not very different (§ 2). One should therefore not ignore the information obtained in crystalline GaAs concerning either transition-metal impurities (e.g. chromium) or intrinsic defects (e.g. the As_{Ga} anti-site defect, where an As atom replaces a Ga atom). Up to now the main interest on the transition metal ions has been on the 3d elements (for reviews see [32, 33]), mainly chromium, which can exist in different oxidation states in GaAs and has been widely used in order to get semi-insulating GaAs. A review of the studies of intrinsic defects in GaAs has recently appeared [34]. Hereafter we will focus particularly on the ESR results about the As_{Ga} defect, because of their possible relevance to our studies. We first note that when a defect consists of an unpaired electron localised around a Ga or As atom, the ESR study is made difficult by the fact that all host nuclei have magnetic moments (table 1), which results in a loss of sensitivity†. If, in an experiment with the usual field modulation and lock-in detection, an electron is strongly coupled to a first nucleus with spin I (which is supposed to lead to a resolved hyperfine structure) and more weakly coupled to other equivalent nuclei (which are supposed to broaden each of hyperfine lines from a value ΔB_0 to a value ΔB), the intensity is lowered by a factor $(2I + 1)(\Delta B/\Delta B_0)$, which can be far greater than one.

The first identification of an antisite defect in a III–V compound was that of P_{Ga} in crystalline GaP [36]. The spectrum (35 GHz, 20 K) consisted of two groups of five hyperfine lines with 1:4:6:4:1 relative intensities (^{31}P: $I = 1/2$, 100% natural abundance. One electron coupled to the central P nucleus, and more weakly to the four ligand P nuclei). The As_{Ga} anti-site spectrum was first found by Wagner and co-workers [37] working at submillimetre frequencies, with $\boldsymbol{B} \parallel [111]$, [110] and [112]. The spectra could be described using an isotropic Zeeman coupling, with $g = 2.04 \pm 0.01$, and an isotropic hyperfine coupling with the central As nucleus, with $|A| = 93.4 \pm 1$ mT (337 GHz) or $|A| = 94.4 \pm 1$ mT (246 GHz). The weaker hyperfine coupling due to the neighbouring As nuclei was not resolved. It was reasoned that the defect could not be Ga_{As}, because the spectra were not compatible with the strong difference existing between the nuclear magnetic moments of ^{69}Ga and ^{71}Ga. The low concentration of defects (8×10^{15} cm^{-3}) did not allow ESR observation at X-band frequencies. Later on, Elliott and co-workers [38] were able to observe this defect at X-band, in bulk SILEC (semi-insulating liquid encapsulated Czochralski) GaAs. Their results were confirmed by Kaufmann and co-workers [39] who, from a study of ten crystals of various origins, concluded that the As_{Ga} defect was systematically present in as-grown SI crystals and was also present in their Bridgman-grown SI sample. The defect was found to be stable up to an annealing temperature of 850 °C. Moreover, it was identified in crystalline GaAs after irradiation by electrons [40], by neutrons [41], and after plastic deformation (static compression at 400 °C) [42]. All these results were obtained with crystalline GaAs. Possible contaminants are transition metal ions [34], boron, carbon, silicon, and sulphur.

† The opposite situation applies in Si, which has only one natural isotope with a magnetic nuclear moment (^{29}Si, $I = \frac{1}{2}$), with a low natural abundancy (4.7%). The ESR of As and P donors in Si were observed early on [35], the lines being narrow.

Table 2. ESR results for the anti-site and other defects in GaAs.

Sample	Treatment	Reference	Anti-site defect			Other defects
			A (MHz)	g	Concentration (cm^{-3})	Concentration (cm^{-3})
Crystalline	—	[37]	2820	2.04	8×10^{15}	Cr-doped
Crystalline	SILEC	[38]			Present	B (10^{16}–10^{17}) C.
Crystalline	SILEC	[39]			Present	Depends on sample (Cr, Fe, Ni, etc.)
Crystalline	Electron irradiation	[40]	2599 ± 35	2.037 ± 0.003	3×10^{16}–2×10^{18}	Si (C, Cr); unidentified line at $g_{eff} = 2.09$ (80 mT)
Crystalline	Neutron irradiation	[41]	2653		3×10^{16}–3×10^{18}	Additional line
Crystalline	Plastic deformation	[42]				
Amorphous	MBD	[43]			Present, mid-10^{17}	
Amorphous	RF sputtering	[44]			Absent	No H: $g_{eff} = 2.07$; 30 mT; 25%H: $g_{eff} = 1.94$; 14 mT
Amorphous	—	[45]			Absent	≃ Stoichiometric: $g_{eff} = 2.06$; As-rich: $g_{eff} = 2.07$, asymmetric, 10^{18} cm^{-3}

Up to now, ESR investigations of amorphous GaAs have been rather scarce and qualitative. Greenbaum and co-workers [43] found the anti-site signal in a sample prepared by molecular beam deposition (MBD). Its concentration was estimated to be in the mid-10^{17} cm^{-3} range. Hoheisel and co-workers [44] studied samples prepared by RF sputtering in Ar with different partial pressures of hydrogen, between 20 and 300 K. At 20 K, they found no anti-site signal. In the sample without hydrogen they found an ESR signal with $g_{eff} = 2.07$ and width 30 mT, while in that with 25% hydrogen atoms, they found another signal with $g_{eff} = 1.94$ and width 14 mT. They suggested that they could perhaps correspond respectively to As and Ga dangling bonds. Von Bardeleben and co-workers [45] have studied the flash-evaporated films mentioned in § 2, in nearly stoichiometric samples (Ga content: 50 ± 2 atoms%). At 6 K, they found an ESR signal with $g_{eff} = 2.06 \pm 0.02$ and width 30 mT, resembling that seen by Hoheisel in unhydrogenated Ar-sputtered a-GaAs. In As-rich samples (Ga content: 40–45 atoms%) they found instead a highly asymmetric line shape with $g_{eff} = 2.07$ and width 23 mT. Assuming $S = \frac{1}{2}$, the spin concentration was found to be 10^{18} cm^{-3} in both cases.

4. Sample preparation, experimental conditions and results

Amorphous films were deposited using a conventional diode RF sputtering system adequately trapped with liquid nitrogen. A water-cooled monocrystalline GaAs target with diameter 5 cm was used. Power input to the target was controlled to give 800 V DC bias. In all cases, prior to the operation, the system was baked and the pre-cleaned glass substrate was thoroughly outgassed at 300 °C. A base pressure of approximately 10^{-6} Torr was obtained. All films were produced with a target-substrate spacing of 3 cm, in a total pressure of 58 mTorr. The films were sputtered in a pure argon atmosphere with the substrate temperature maintained at 30 °C. The amorphicity of the films was checked by means of x-ray diffraction analysis and their compositions were determined from micro-analysis of x-ray emissions.

Three samples were produced, from three separate periods (2–3 h each) in the same sputtering run. The aim was to prevent any crystallisation happening during long sputtering processes. The substrate was a glass plaque on which a B_2O_3 thin film had been evaporated. The a-GaAs substance was removed by immersion in distilled water. The resulting a-GaAs plaques were then washed, dried and packed in a quartz ESR tube. The mass of a-GaAs used in the ESR experiments was 14.6 mg.

The experiments were performed with an X-band spectrometer (Varian E112) at 9.4 GHz with a variable temperature gas-flow cryostat (Oxford ESR9). The intensity measurements of the resonance signal were made by comparing the signal from the sample at the temperature of the experiment (3.9 K) with that given by a reference sample (strong pitch) at room temperature, using a double rectangular cavity. In the experiments the usual field modulation and lock-in detection were used, and the derivative of the absorption was recorded. The output of the spectrometer was coupled to a computer (Nova 4 from Data General) which performed a first numerical integration, leading to the absorption signal, and a second integration giving the area under the absorption curve. This double integration was carried out for both the a-GaAs and the reference samples. When choosing the amplitude of the field modulation and the RF power, care was taken to avoid overmodulation of the ESR lines and partial saturation. In order to get the number of spins from these results, it is necessary to know the value of the spin of the paramagnetic centres, and the absorption law. We will consider this

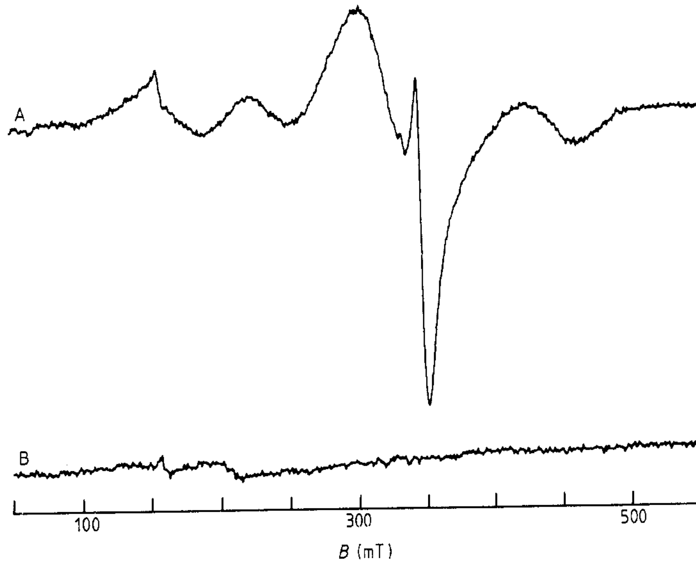

Figure 1. Curve A, ESR spectrum of an amorphous GaAs sample (14.4 mg) prepared by RF sputtering. (9375 MHz; $T = 3.9$ K; field modulation; 4 mT peak-to-peak; RF power; 0.1 mW). Curve B, spurious contribution from the cavity and tube under the same conditions.

point together with our experimental results. The field values were obtained from the Varian Hall probe, and the calibration was checked with the pitch resonance signal. The ESR signal from the sample at 3.9 K is presented in curve A of figure 1. The spurious contribution of the cavity and empty tube to this signal is weak (curve B), and the true ESR signal, obtained after subtraction of this spurious contribution, is given in figure 2. This signal originates from three different centres which we call 1, 2 and 3. Their origin will be discussed in § 5.

(i) Signal 1 consists of four almost equidistant lines. It can be described by a spin Hamiltonian $h = g\beta BS_2 + AS \cdot I$, with $S = \frac{1}{2}$, $I = \frac{3}{2}$, $g = 2.06 \pm 0.01$, $A/g\beta = 89.9 \pm 0.5$ mT. Assuming a Curie law, we find a 7×10^{17} cm^{-3} concentration. We will attribute signal 1 to the As_{Ga}^{+} anti-site defect (§ 5.1), and recent results [46] then confirm our assumption for $\chi(T)$.

(ii) Signal 2 consists of a single broad line ($\Delta B_{pp} = 47.5$ mT) centred at $g_{eff} = 2.058 \pm 0.004$. Assuming $S = \frac{1}{2}$ and a Curie law we find a concentration of 8×10^{17} cm^{-3}. Within experimental accuracy, this value is the same as that of signal 1. We think this is not fortuitous, and in § 5 we shall postulate that both centres have the same origin.

(iii) Signal 3 consists of a single narrower line ($\Delta B_{pp} = 7.5$ mT) centred at $g_{eff} = 1.925 \pm 0.002$. Assuming $S = \frac{1}{2}$ and a Curie law we find a concentration of 0.4×10^{17} cm^{-3}. The origin of this signal is uncertain, as will be discussed in § 5.5.

Figure 3, curve C shows the derivative of a Lorentzian curve with centre and width chosen to fit the contribution attributed to signal 3 in the experimental spectrum. Figure 3, curve B similarly corresponds to the derivative of a Lorentzian curve compatible with signal 2. The dotted curve in figure 2 is obtained by superposing curves A, B, C of figure 3 with curve C chosen to give as close a fit to the experimental results as possible. The values for the width ΔB_{pp} and the positions g_{eff} were determined from figure 3 curves A,

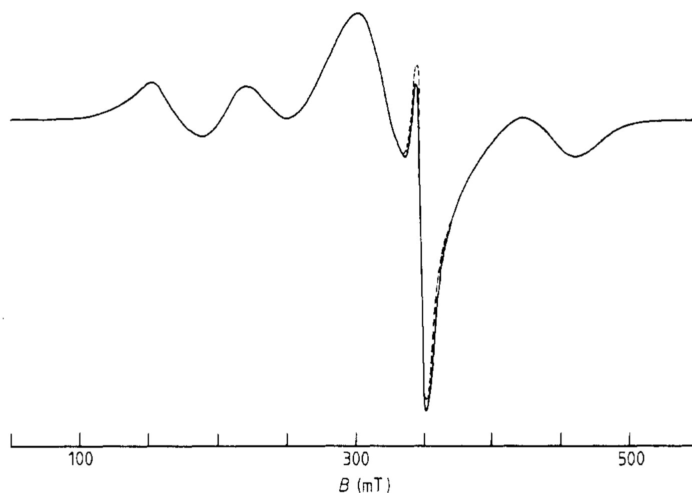

Figure 2. Full curve, the ESR spectrum of figure 1, curve A, after subtraction of the spurious contribution shown in figure 1, curve B; the broken curve represents the sum of the contributions attributed to the different centres (see figure 3).

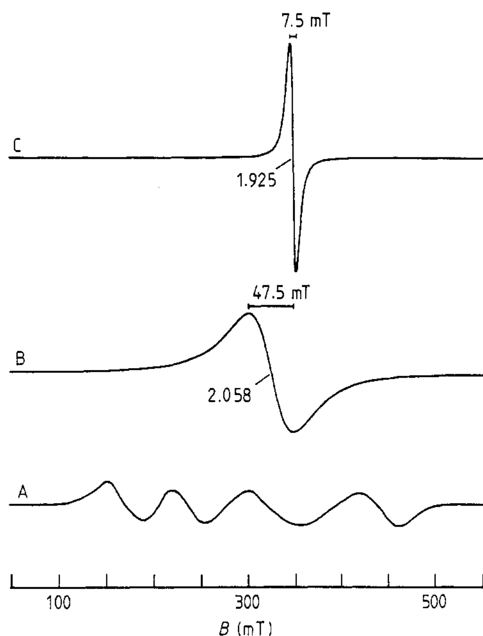

Figure 3. Curve C, derivative of a Lorentzian line simulating the contribution from signal 3. Curve B, derivative of a Lorentzian line simulating the contribution from signal 2. Curve A, corresponds to signal 1. Superposition of curves A, B, C is given in figure 2, together with the experimental result. Curve A was chosen to give as close a fit to the experimental result as possible.

B and C. However the results are very similar to that obtained with the experimental spectrum (figure 1), and the main purpose of figure 3 curve C is in visualising the different contributions, and so aid in the discussion of signal 1.

5. Discussion

5.1. Determination of A- and g-values for signal 1

Signal 1 is composed of four lines with nearly equal intensities, which look like hyperfine structured lines. The coupling of the hyperfine structure is evidently strong and in

consequence the lines are not strictly equidistant. Also, remembering that the sample is isotropic, the relatively small linewidths suggest that the electron–nucleus coupling is mainly isotropic and therefore probably due to an unpaired s electron. We shall first consider the positions of the resonance lines, rather than their widths. We assume that all the ions have the same isotropic g-value, and examine the question of the linewidth later on (§ 5.4). The spin-Hamiltonian is

$$h = g\beta BS_z + AS_zI_z + \tfrac{1}{2}A(S^+I^- + S^-I^+) \qquad S = \tfrac{1}{2}, I = \tfrac{3}{2}.$$

In the basis of the eight $|M_S, M_I\rangle$ states, the matrix of this spin-Hamiltonian separates into two one-dimensional and three two-dimensional submatrices, and its eigenvalues and eigenstates can be found exactly. The one-dimensional matrices are spanned by the $|\tfrac{1}{2}, \tfrac{3}{2}\rangle$ and $|-\tfrac{1}{2}, -\tfrac{3}{2}\rangle$ states respectively. The spaces of the two-dimensional matrices are spanned by the following states: $|\tfrac{1}{2}, \tfrac{1}{2}\rangle$ and $|-\tfrac{1}{2}, \tfrac{3}{2}\rangle$, $|\tfrac{1}{2}, -\tfrac{1}{2}\rangle$ and $|-\tfrac{1}{2}, \tfrac{1}{2}\rangle$, $|\tfrac{1}{2}, -\tfrac{3}{2}\rangle$ and $|-\tfrac{1}{2}, -\tfrac{1}{2}\rangle$. We shall call $|\varphi_{M_S, M_I}\rangle$ the corresponding eigenstates; for instance the eigenstates corresponding to the subspace spanned by $|\tfrac{1}{2}, \tfrac{1}{2}\rangle$ and $|-\tfrac{1}{2}, \tfrac{3}{2}\rangle$ are $|\varphi_{1/2,1/2}\rangle$ and $|\varphi_{-1/2,3/2}\rangle$ and, when $A/g\beta B \rightarrow 0$, $|\varphi_{1/2,1/2}\rangle \rightarrow |\tfrac{1}{2}, \tfrac{1}{2}\rangle$ while $|\varphi_{-1/2,3/2}\rangle \rightarrow |-\tfrac{1}{2}, \tfrac{3}{2}\rangle$. Putting $A' = A/g\beta$ and $B_0 = h\nu/g\beta$, where ν is the frequency of the RF field (kept constant in the experiment; in our measurements ν was 9.375 GHz), the resonance fields for the different transitions, called B instead of $B_1, \ldots, B_4$ for brevity, are as follows:

$$|\tfrac{1}{2}, \tfrac{3}{2}\rangle \rightarrow |\varphi_{-1/2,3/2}\rangle \qquad B_0 = \tfrac{1}{2}\sqrt{B^2 + 2BA' + 4A'^2} + \tfrac{1}{2}B + A' \tag{1}$$

$$|\varphi_{1/2,1/2}\rangle \rightarrow |\varphi_{-1/2,1/2}\rangle \qquad B_0 = \tfrac{1}{2}(\sqrt{B^2 + 2BA' + 4A'^2} + \sqrt{B^2 + 4A'^2}) \tag{2}$$

$$|\varphi_{-1/2,-1/2}\rangle \rightarrow |\varphi_{-1/2,1/2}\rangle \qquad B_0 = \tfrac{1}{2}[\sqrt{B^2 - 2BA' + 4A'^2} + \sqrt{B^2 + 4A'^2}] \tag{3}$$

$$|\tfrac{1}{2}, -\tfrac{3}{2}\rangle \rightarrow |\varphi_{-1/2,-3/2}\rangle \qquad B_0 = \tfrac{1}{2}\sqrt{B^2 - 2BA' + 4A'^2} + \tfrac{1}{2}B - A'. \tag{4}$$

The experimental values of the resonance fields are 168.0, 237.4, 323.0 and 443.0 mT. A' and g are found from (1) and (4). However, when this value of A' is used in (2) and (3), slightly different g-values are obtained. Perfect agreement is not expected because of experimental errors, particularly in the resonance field for the line near 240 mT. Overall the agreement is really quite satisfactory, using $A' = 89.9 \pm 0.5$ mT and $g = 2.06 \pm 0.01$. From now on we will write A instead of A' as usual.

5.2. *Origin of signal 1*

The g- and A-values for signal 1, namely $g = 2.06 \pm 0.01$ and $A = 89.9 \pm 0.5$ mT, are very similar to those found by Wagner and co-workers [37] for the anti-site defect in crystalline GaAs ($g = 2.04 \pm 0.01$ and $A = 93.4 \pm 1$ mT or 94.4 ± 1 mT (cf § 3)). We are therefore convinced that signal 1 is produced by the anti-site defect. There is a slight difference for the A-values in the two materials, which only means that the probability density of the electron at the nucleus is slightly different ($\simeq 5\%$) in crystalline GaAs from that in our amorphous material.

It is easier to discuss first the formation of this defect in the crystalline material, beginning by considering the bonds between Ga and As atoms in the crystal without defect. We shall adopt the point of view followed by Bates and Stevens [33]. Since gallium has three valence electrons (ground configuration $4s^2\,4p^1$) and arsenic five (ground configuration $4s^2\,4p^3$), and both are surrounded by a tetrahedron of opposite

atoms, it is natural to assume that as a first step each arsenic atom gives up an electron to a gallium atom. Each ion is then isoelectronic with germanium and the description usually used for Si or Ge is valid. However, the electron will be nearer to the positively charged arsenic than to the gallium, which will partially neutralise the charges of the ions. GaAs has only a slight ionic character. If an arsenic atom replaces a gallium atom (anti-site defect), there are two extra electrons. Here it is relevant that GaAs often contains impurities like chromium, introduced in order to compensate the material. This was the case in the samples used by Wagner and co-workers [37] when they found the anti-site defect. It is therefore probable that as a first step one electron will be lost by the arsenic and taken by a chromium ion (which can exist as Cr^{2+}, Cr^{3+} or Cr^{4+}). If this electron had been in the conduction band, the material in [37] would have conducted. In fact it was semi-insulating. Moreover, a Cr^{2+} signal was observed. The remaining electron will be attracted by two positive charges (As_{Ga}^{+} defect). We now come to the situation in the amorphous sample. Amorphous GaAs is generally not strictly stoichiometric, and in the present case we have an As excess (the proportion of As is not 0.50 but 0.54 ± 0.01). The simplest way to reconcile this As excess with the idea that each atom is in a tetrahedral configuration (§ 2) is to imagine the existence of As atoms at the Ga sites, i.e. anti-site defects. What is surprising is not the presence of the anti-site defect, but that its concentration (3×10^{-5} defects/As atom) is lower than expected. How are the other excess As atoms placed? A possibility could be that for these atoms the tetrahedral configuration is not achieved locally, the excess arsenic having fivefold coordination as in the Kolomiets–Mott mechanism in amorphous solids ([2] p 44). P can exist in fivefold configuration, for instance in PCl_5 [47], and compounds with As in fivefold coordination are also known (for instance AsF_5 [48]).

5.3. *Discussion of the g- and A-values of signal 1*

We first discuss the origin of Δg, the shift of g from the free-spin value. GaAs is a tetrahedral covalent compound, and the existence of the bands in the crystalline solid can be predicted using the tight-binding approximation (§ 2). A model appropriate for the description of the As_{Ga} point defect will therefore use a molecule with T_d symmetry, with O, the central substitutional arsenic, at the centre of the tetrahedron, and A, B, C, D, the arsenic ligands, at the apices (figure 4), and the LCAO method for the description of the molecular orbitals (MO) [49] (a crystal field description would use the strong-field approximation [50]). We use the 4s, $4p_x$, $4p_y$, $4p_z$ atomic orbitals (AO) for the central atom. The present situation—a point defect in a solid—is more complex than a true molecule, which is apparent on writing down the orbitals for the ligands. For the A ligand, we choose $(\lambda s + \mu p_{AO})_A$, where s is the 4s orbital centred on A, and $p_{AO} = (1/\sqrt{3})(p_x - p_y - p_z)$ is a hybrid orbital directed along AO, and built from the $4p_x$, $4p_y$, $4p_z$ AO of the A ligand defined with local axes parallel to those used for the central atom (figure 4). We choose similar hybrids for the other ligands, and give their expressions in figure 4. This choice is consistent with the idea that in GaAs the bonding orbitals correspond to sp^3 hybridisation. Since we will consider only one orbital state for each ligand, which is symmetrical about the line joining the ligand to the central ion, we are in a well known situation, first studied by VanVleck [51, 52]. The functional space of the AO is the direct sum of two invariant subspaces, the first of which is spanned by s, p_x, p_y, p_z of the central atom, and which defines the reducible representation Γ_M ($\Gamma_M = A_1 + T_2$). Neglecting overlap, the antibonding orbitals are

$$A_1: \cos\alpha(4s)_O + [\sin\alpha/\sqrt{4(\lambda^2+\mu^2)}] \times [(\lambda s + \mu p_{AO})_A + (\lambda s + \mu p_{BO})_B + (\lambda s + \mu p_{CO})_C + (\lambda s + \mu p_{DO})_D)]$$

$$T_2:\begin{cases}\cos\beta(4p_x)_O + [\sin\beta/\sqrt{4(\lambda^2+\mu^2)}] \\ \quad \times[-(\lambda s+\mu p_{AO})_A + (\lambda s+\mu p_{BO})_B + (\lambda s+\mu p_{CO})_C - (\lambda s+\mu p_{DO})_D)] \\ \cos\beta(4p_y)_O + [\sin\beta/\sqrt{4(\lambda^2+\mu^2)}] \\ \quad \times[+(\lambda s+\mu p_{AO})_A - (\lambda s+\mu p_{BO})_B + (\lambda s+\mu p_{CO})_C - (\lambda s+\mu p_{DO})_D] \\ \cos\beta(4p_z)_O + [\sin\beta/\sqrt{4(\lambda^2+\mu^2)}] \\ \quad \times[+(\lambda s+\mu p_{AO})_A + (\lambda s+\mu p_{BO})_B - (\lambda s+\mu p_{CO})_C - (\lambda s+\mu p_{DO})_D].\end{cases}$$

The bonding orbitals are obtained by changing α into $\alpha + \frac{1}{2}\pi$ and β into $\beta + \frac{1}{2}\pi$. The discussion of § 5.2 shows that nine electrons have to be placed into these orbitals. Eight occupy the four bonding orbitals, leaving one in an antibonding orbital. The existence of a hyperfine structure with a high A-value indicates that the electron is in the $(4s)_O$ type antibonding orbital (that with A_1 symmetry). $\Delta g = +0.06$, the shift from the g-value of the free spin, is due to spin–orbit coupling. Spin–orbit cannot couple A_1 to A_1 so Δg is due to a coupling of the A_1 orbital to the T_2 orbitals which is not possible unless the spin–orbit is due to ligands. Since we deal with tetrahedral symmetry, g is isotropic, and $\Delta g = \Delta g_{ZZ}$. Δg is due to second-order processes. Using the strong-field formalism [50], the ground state is $t_2^6a_1^2a_1^*$, and possible intermediate states are (figure 5) $t_2^6a_1^2t_2^*$ (promotion of the lone electron to an empty orbital) or $t_2^5a_1^2a_1^{*2}$ (promotion of an electron from a filled orbital). The spin–orbit (SO) coupling should not be taken as $\Sigma\zeta(r)\, \boldsymbol{l}_i \cdot \boldsymbol{s}_i$ (there is no spherical symmetry) but as $\Sigma \boldsymbol{t}_i \cdot \boldsymbol{s}_i$, where $\boldsymbol{t}_i$ transforms like a (pseudo)vector under the symmetry operations of T_d, the symmetry group of the molecule. We write it $\Sigma\zeta' \boldsymbol{l}_i \cdot \boldsymbol{s}_i$ (ζ' is not the SO constant of the free atom; in crystalline GaAs the SO splitting of the bands is 0.33 eV [53]). The matrix elements of $\beta B L_z$ and $\Sigma\zeta' l_{zi}s_{zi}$ between the Slater determinants are simplified by noting that the SO coupling is a sum of one electron operators, and one finally obtains (appendix 1):

$$\Delta g_{zz} \simeq 2\zeta'[-|\langle a_1^*|l_z|t_2^{*z}\rangle|^2/\Delta_1 + |\langle t_2^z|l_z|a_1^*\rangle|^2/\Delta_2].$$

Promotion of an electron into the empty higher t_2^{*z} orbital is responsible for the first term in the brackets and gives a negative Δg. Promotion of an electron from the filled t_2^z orbital into the partially filled a_1^* orbital is responsible for the second term and gives a positive Δg [54]. The observed positive Δg suggests that the dominant mechanism is the promotion of an electron from a bonding orbital.

We now examine the hyperfine coupling. For As_{Ga}, we have found that $A/g\beta = 89.9$ mT and $g = 2.06$, i.e. $A = 2590$ MHz. The nuclear magnetic moment may be magnetically coupled to the electron in three different ways: (i) with the magnetic field induced by the orbital motion of the electrons (coupling to $\boldsymbol{L}$), and with the electron spin; (ii) dipole–dipole coupling; and (iii) Fermi contact term. In the $^4S_{3/2}$ ground term of the $4s^24p^3$ ground configuration of the neutral atom, the magnetic hyperfine coupling is theoretically zero [55, 56]. A weak hyperfine coupling has been found experimentally in arsenic vapour (−66.2 MHz) [57], and with arsenic atoms diluted into an inert krypton matrix (31.3 MHz) [58], and is attributed to the configuration interaction. We have observed a far stronger coupling, which confirms that in the As_{Ga}^+ defect the arsenic is not in the ^4S ground state of the neutral atom. From experimental values collected in Landolt–Börnstein [59], one can deduce (appendix 2) that, in the ^4D term of the sp^3 configuration of As, there exists a weak contribution from $\boldsymbol{L}$ (330 MHz) and, as expected, a strong contribution from $\boldsymbol{S}$ (6625 MHz). However, a direct comparison of our experimental A-value with this last one is questionable, since in the As_{Ga}^+ defect arsenic is in

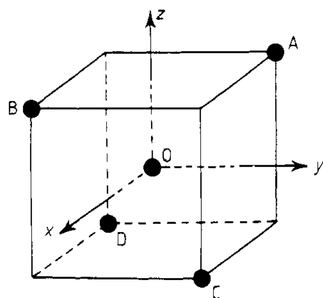

Figure 4. The model for the anti-site defect, with a central arsenic atom and four arsenic neighbours in T_d symmetry. The relations expressing p_{XO} (X = A, B, C, D), the hybrid orbital centred on ligand X, in terms of atomic p orbitals are $p_{AO} = (1/\sqrt{3})(p_x - p_y - p_z)$, $p_{BO} = (1/\sqrt{3})(-p_x + p_y - p_z)$, $p_{CO} = (1/\sqrt{3})(-p_x - p_y + p_z)$, and $p_{DO} = (1/\sqrt{3})(p_x + p_y + p_z)$. In these expressions, local axes centred on X and parallel to Ox, Oy, Oz respectively are used.

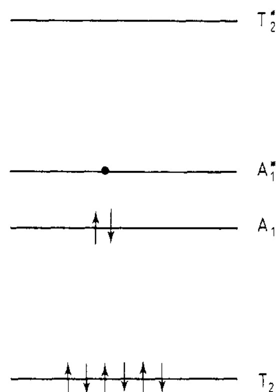

Figure 5. The MO energy diagram for the As_{Ga}^+ defect.

a strong ligand field. We have therefore preferred to compare it with the theoretical A-value due to the contact term from an electron entirely in an s state in arsenic; this comparison gives the value of $\cos^2 \alpha$, i.e. the proportion of the s state in the A_1 antibonding orbital. It is known [60] that Froese's Hartree–Fock wavefunctions sometimes yield spin densities in excess of unity. Morton and Preston [60] have examined this problem and produced a tabulation of $\Psi^2(0)$ and $\langle r^3 \rangle$ values obtained from the Hartree–Fock–Slater AO of Hermann and Skillman. For As, they obtain $A = 14\,660$ MHz for unit spin density in the 4s orbital. We therefore conclude that the A_1 antibonding orbital has 17.7% s character ($\cos \alpha = 0.42$), and that the electron spends ≈20% of its time on each of the four ligands. We will be able to get additional information upon the ligand part of the wave function by examining the width of the ESR lines of signal 1. We should, however, stress that our experimental A-value is far greater than that of As donors in Si [35] (7.3 mT). In the anti-site defect, the wavefunction is concentrated around the central arsenic and first ligands (deep level), while it is quite delocalised in Si (shallow donor).

5.4. *The origin of the width of the As_{Ga} ESR lines*

The experimental peak-to-peak linewidth is $\Delta B_{pp} \simeq 39$ mT, and can be approximated by the derivative of a Gaussian† function, whose width at half height, $\Delta B_{1/2} = 1.18\Delta B_{pp}$, is 46 mT. The width cannot come from the fluctuations of the g-value from site-to-site, since the ligand field affects the g-value only weakly (the mean Δg shift from the free-spin value is only 0.06, corresponding to 9.6 mT). An estimate of the dipolar width, using simplifying assumptions, suggests that this is not the origin either. Suppose that

† We recall that the assumption of a Lorentz shape was made for signals 2 and 3, not for signal 1, which was obtained by subtracting the derivative of Lorentz functions (figure 3 curves B and C) from the experimental spectrum.

the Ga *sites* are regularly distributed on a simple cubic lattice (the volume per Ga site being the same as in crystalline GaAs: 45.5 $Å^3$), each Ga site being occupied by an As atom with a probability f ($f = 8 \times 10^{17}/2.2 \times 10^{22} \simeq 4 \times 10^{-5}$). We use the Van Vleck method of moments and the treatment from Kittel and Abrahams for dilute systems [61] for $S = \frac{1}{2}$ spins. δ, the linewidth, is $\delta = 5.3 g^2\beta^2/a^3$, a being the distance between nearest-neighbouring Ga sites in the model lattice ($a^3 = 45.5$ $Å^3$) (we have ignored the existence of the nuclear spin). The theoretical width of the absorption line is then only $\delta \simeq 0.01$ mT. This leaves the possibility that the width is due to the coupling of the electron with the four equivalent arsenic ligand nuclei, which is quite reasonable since the corresponding part of the wavefunction has an s contribution. The associated Hamiltonian is $A_L S_z \Sigma I_{z,L}$, where A_L is the hyperfine coupling constant, $I_{z,L}$ being the z component of $\boldsymbol{I}$ for ligand L. It is easy to show that the weights of the 4^4 different M_I-states (with M_I ranging from -6 to $+6$) are 1:4:10:20:31:40:44:40 . . . 1. Such an unresolved pattern gives a Gaussian line with width at half height, $\Delta H_{1/2} = 5.37 A_L$, leading to $A_L = 248$ MHz. The hyperfine coupling with a given ligand nucleus has in fact both a contact (s-part) and a dipole–dipole (p-part) contribution. Since the hyperfine coupling is far weaker than the Zeeman coupling, one can neglect the x and y components of $\boldsymbol{S}$ and $\boldsymbol{I}$ in the dipolar Hamiltonian (Oz being taken along the applied field $\boldsymbol{B}$) and finally [62]

$$A \simeq A_{iso} + B(3\cos^2\theta - 1)$$

where A_{iso} is the isotropic, contact term and θ the angle between $\boldsymbol{B}$ and the axis of the p orbital. The resonance condition is

$$h\nu = g\beta B + [A_{iso} + B(3\cos^2\theta - 1)]M_I \qquad (M_I = -6, \ldots, +6).$$

We consider a given M_I. Because of the dipolar term, the corresponding line will be broadened and/or shifted. We assume, as is usual for a powder spectrum, that all the directions have the same probability. The form factor of the line associated with a given M_I will be $f(H) \propto 1/\cos\theta$. $f(H)$ is a maximum for $\theta = \frac{1}{2}\pi$, and the corresponding dipolar contribution is $-B$. Since at this level of approximation $f(H)$ diverges for $\theta = \frac{1}{2}\pi$, the main effect of the dipole–dipole term is to shift the resonance so that $A_L \simeq A_{iso} - B$. Morton and Preston [60] have tabulated the B-values. For ^{75}As and an electron in a p state, $B = 334$ MHz. From these data and those of § 5.3, we obtain

$$(0.908^2/4)[(\lambda^2/\lambda^2 + \mu^2)14660 - (\mu^2/\lambda^2 + \mu^2)334] = 248$$

The part of the A_1 wavefunction associated with a given ligand is therefore $(0.908/\sqrt{4})[0.32\mathrm{s} + 0.947\mathrm{p}]$, which means that this part of the wavefunction is mainly of p character (the ratio, $\lambda^2/\mu^2 = 0.114$, would be $\frac{1}{3}$ for a pure sp^3 orbital). It is gratifying to observe that a fairly similar result was observed [63] with P_{Ga} in crystalline GaP ($\lambda^2/\mu^2 = 0.136$ and $I = \frac{1}{2}$, the structure due to the ligand nuclei being well resolved—see [36] and § 3—which made the determination of λ and μ more precise). From all the above (cf § 2), we can safely conclude that our results for the wavefunction of the As_{Ga}^{+} defect are consistent with those for the crystalline material.

5.5. *Origin of signals 2 and 3*

Since we have found the same concentration for the centre corresponding to signal 2 as for signal 1, it is natural to consider that signal 2 corresponds to the capture of the first electron. We are not able to identify the defect responsible for its capture. We note that

if its concentration was greater than that of the As_{Ga} defect, it could act as a trap for electrons of deliberately introduced donors.

Signal 3 can be attributed to a centre with $S = \frac{1}{2}$ and $g = 1.925 \pm 0.002$. We think that this defect is not the same as that observed by Hoheisel (cf § 3, table 2), not because of the difference in $(g - 2)$ values (15%), but because Hoheisel obtained it in the presence of hydrogen. For a similar reason we think that this centre is not that detected by Baeumler and co-workers [64] ($g = 1.94$), because their signal only appeared after prolonged irradiation with 1.18 eV photons. This led to a quenching of the As^{+}_{Ga} photo-induced signal, while our defect coexists with the As^{+}_{Ga} one, and has a smaller concentration. Since our material has a strong As excess, one might think that it is also an As defect, but this is not compatible with the absence of hyperfine structure. Nor do we think that it is related to a dangling bond, as one would then expect to detect the hyperfine structure from either As or Ga (or both) (see for instance the case of the dangling bonds in amorphous Si [65]). It seems therefore more likely that signal 3 is related to a chemical impurity. Assuming that the g-value is the same in crystalline and amorphous GaAs, which is compatible with the idea that the local order is maintained in amorphous GaAs, we finally note that none of the 3d impurities in GaAs reviewed in [32] are good candidates. Clearly more study will be necessary for its identification.

6. Conclusion

We have used ESR for a study of the paramagnetic centres in amorphous films prepared by RF sputtering. We were able to detect the anti-site defect with a concentration of 7×10^{17} cm^{-3}. This result is clearly compatible with previous results obtained with flash evaporated samples and described in § 3 showing that like-atom bonds are unlikely, so implying that their concentration was less than about 1%. Using the positions and widths of the ESR lines from the As^{+}_{Ga} defect, we found that the paramagnetic electron is in an A_1 state, that the central atom part of the wavefunction has about 18% s-character, and that the s-character for one ligand is 10% of the remaining part, neglecting the contribution from the second neighbours. We have found that the positive Δg comes from the promotion of an electron from a filled bonding orbital into partially filled anti-bonding orbital. We have shown that one of the excess electrons of the arsenic is taken by a nearby defect and can be detected by ESR, which indicates the presence of electron traps. We have found a third centre with a lower concentration (0.4×10^{17} cm^{-3}) which probably indicates the presence of some unidentified chemical impurity. It would be of interest to study the ESR behviour of the material under optical irradiation, and after treatment in a hydrogen flow.

Appendix 1. Δg_{zz} determination

We call $|0\rangle$ the Slater determinant (SD) corresponding to one of the states of the $t_2^6 a_1^2 a_1^*$ ground doublet

$$|0\rangle = \{\overset{+}{t}{}_2^x \overset{-}{t}{}_2^x \overset{+}{t}{}_2^y \overset{-}{t}{}_2^y \overset{+}{t}{}_2^z \overset{-}{t}{}_2^z \overset{+}{a}_1 \overset{-}{a}_1 \overset{+}{a}{}_1^*\}$$

We first consider the determination of Δg_{zz} when the intermediate state, called $|1\rangle$, corresponds to the promotion of the a_1^* electron to the empty t_2^* level (in fact, as will be shown later, to the $\overset{+}{t}{}_2^{*z}$ state). $|1\rangle$ is the SD obtained by replacing $\overset{+}{a}{}_1^*$ by $\overset{+}{t}{}_2^*$ in $|0\rangle$ (the

order of the one electron functions in the definition of $|1\rangle$, and later on of $|2\rangle$, is chosen to avoid permutations in the calculations of the matrix elements). The energy correction is

$$-(\beta B/\Delta_1)\,[\langle 0|L_z|1\rangle\langle 1|\Sigma\zeta' l_z s_z|0\rangle + \langle 0|\Sigma\zeta' l_z s_z|1\rangle\langle 1|L_z|0\rangle] \qquad \text{(A1.1)}$$

where $\Delta_1 = E_1 - E_0$ (E_0 = energy of $|0\rangle$; E_1 = energy of $|1\rangle$). Using the simplification introduced by the fact that the operators are both a sum of one-electron operators, one gets:

$$\langle 0|L_z|1\rangle = \langle \overset{+}{a}{}_1^*|l_z|\overset{+}{t}{}_2^*|\rangle = \langle a_1^*|l_z|t_2^*\rangle$$

where $|a_1^*\rangle$, $|t_2^*\rangle$ and l_z are one-electron quantities. One could *a priori* consider t_2^{*x}, t_2^{*y} or t_2^{*z}; in fact, since l_z transforms as z under the operations of T_d, it can couple a_1^* to t_2^{*z}; in the same way

$$\langle 1|\Sigma t_z s_z|0\rangle = \langle \overset{+}{t}{}_2^*|t_z s_z|\overset{+}{a}{}_1^*\rangle = \langle t_2^*|t_z|a_1^*\rangle\langle +|s_z|+\rangle.$$

We consider that $t_z \simeq l_z$; the energy correction is therefore approximately

$$(2\beta B\zeta/\Delta_1)|\langle a_1^*|l_z|t_2^{*z}\rangle|^2(+\tfrac{1}{2}) \qquad \Delta g_{zz} \simeq -(2\zeta/\Delta_1)|\langle a_1^*|l_z|t_2^{*z}\rangle|^2 < 0.$$

We now consider the determination of Δg_{zz} when the intermediate state corresponds to the promotion of an electron from the t_2 filled level to the a_1^* level. $|2\rangle$ is the SD obtained by replacing $\bar{t}_2^z$ by $\bar{a}_1^*$ in $|0\rangle$ (the same selection rule as before precludes t_2^x and t_2^y); the energy correction is obtained by replacing $|1\rangle$ by $|2\rangle$ and Δ_1 by Δ_2 in (A1.1), with $\Delta_2 = E_2 - E_1$ (E_2, energy of $|2\rangle$), and now

$$\langle 0|L_z|2\rangle = +\langle \bar{t}_2^z|l_z|\bar{a}_1^*\rangle = \langle t_2^z|l_z|a_1^*\rangle$$

$$\langle 2|\Sigma t_z s_z|0\rangle = +\langle \bar{a}_1^*|t_z s_z|\bar{t}_{2z}\rangle = \langle a_1^*|t_z|t_2^z\rangle\langle -|s_z|-\rangle.$$

The energy correction is now approximately

$$-(\beta B\zeta/\Delta_2)2|\langle t_2^z|l_z|a_1^*\rangle|^2(-\tfrac{1}{2}) \qquad \Delta g_{zz} \simeq +(2\zeta/\Delta_2)|\langle t_2^z|l_z|a_1^*\rangle|^2 > 0.$$

Appendix 2. Hyperfine coupling within the ^{3}D term

Within a ^3D_J multiplet of the sp^3 configuration of As(II), the contribution of the hyperfine coupling to the energy is given [59] by the expression

$$(a(J)/2)[F(F+1) - I(I+1) - J(J+1)]$$

and

$$a(3) = 81 \times 10^{-3}\ \text{cm}^{-1} \qquad \text{(A2.1)}$$

$$a(2) = 46 \times 10^{-3}\ \text{cm}^{-1} \qquad \text{(A2.2)}$$

($\boldsymbol{J} = \boldsymbol{L} + \boldsymbol{S}, \boldsymbol{F} = \boldsymbol{I} + \boldsymbol{J}$).

The hyperfine coupling comes from $\boldsymbol{L}$ and $\boldsymbol{S}$

$$\mathcal{H} = c\boldsymbol{I}\cdot\boldsymbol{S} + d\boldsymbol{I}\cdot\boldsymbol{L}.$$

Within a given J multiplet $\boldsymbol{S} = \alpha\boldsymbol{J}$ and $\boldsymbol{L} = \beta\boldsymbol{J}$, where α (β) depends upon $\boldsymbol{J}$ but not

upon M_s (M_L) (Wigner–Eckart theorem). Therefore

$$\mathcal{H} = (\tfrac{1}{2}c\alpha + \tfrac{1}{2}d\beta)[2\boldsymbol{IJ}]$$

Let us first determine α and β within $^3D_3$. From

$$\alpha J_z|J = 3, M_J = 3\rangle = S_z|L = 2, M_L = 2, S = 1, M_s = 1\rangle$$

one gets $\alpha = \frac{1}{3}$, $\beta = \frac{2}{3}$. From (A2.1) one therefore gets

$$\tfrac{1}{3}c + \tfrac{2}{3}d = 81 \times 10^{-3}\ \mathrm{cm}^{-1}. \qquad \text{(A2.3)}$$

In a similar way we first determine α' and β', the α- and β-values within the $^3D_2$ multiplet. In order to obtain them, we let the lowering operators $J^- = L^- + S^-$ act upon the previous state, which leads to:

$$|J=3, M_J=2\rangle = \sqrt{\tfrac{2}{3}}|L=2, M_L=1, S=1, M_s=1\rangle + \sqrt{\tfrac{1}{3}}|L=2, M_L=2, S=1, M_s=0\rangle$$

$|J=2, M_J=2\rangle$ is orthogonal to this state:

$$|J = 2, M_J = 2\rangle = \sqrt{\tfrac{1}{3}}|L = 2, M_L = 1, S = 1, M_s = 1\rangle - \sqrt{\tfrac{2}{3}}|L = 2, M_L = 2, S = 1, M_S = 0\rangle$$

By taking the mean value of $\alpha' J_z = S_z$ within this state, one gets $\alpha' = \frac{1}{6}$; similarly, using $\beta' J_z = L_z$ one obtains $\beta' = \frac{5}{6}$. Equation (A2.1) leads then to:

$$\tfrac{1}{6}c + \tfrac{5}{6}d = 46 \times 10^{-3}\ \mathrm{cm}^{-1} \qquad \text{(A2.4)}$$

(A2.2) and (A2.3) lead to $c = 221 \times 10^{-3}\ \mathrm{cm}^{-1}$, $d = 11 \times 10^{-3}\ \mathrm{cm}^{-1}$. Therefore, within the ^3D term, the nucleus is coupled mainly to $\boldsymbol{S}$ (6630 MHz), and slightly to $\boldsymbol{L}$ (330 MHz).

References

[1] Ziman J M 1979 *Models of Disorder* (Cambridge: CUP)
[2] Mott N F and Davies E A 1979 *Electronic Processes in Non-crystalline Materials* 2nd ed (Oxford: Clarendon)
[3] *Amorphous Solids, Low-temperature Properties* 1981 ed. W A Philips (Berlin: Springer)
[4] *Ill-condensed matter, Les Houches Session XXXI* 1978 ed. R Balian, R Maynard and G Toulouse (Amsterdam: North Holland)
[5] Connell G A N and Street R A 1980 *Materials, Properties and Preparations* (*Handbook on Semiconductors* 3) vol ed. S P Keller (Amsterdam: North Holland) pp 689–801
[6] Spear W E and Le Comber P G 1975 *Solid State Commun.* **17** 9
[7] Spear W E and Le Comber P G 1976 *Phil. Mag.* **33** 935
[8] Paul W, Lewis A J, Connell G A N and Moustakas T D 1976 *Solid State Commun.* **20** 969
[9] Guinier A 1978 *Ill-condensed matter, Les Houches Session XXXI* 1978 ed. R Balian, R Maynard and G Toulouse (Amsterdam: North Holland) p 485
[10] Cargill G S 1976 *Ann. N.Y. Acad. Sci.* **279** 208.
[11] Polk D E and Boudreaux D S 1973 *Phys. Rev. Lett.* **31** 92
[12] Polk D E 1971 *J. Non-Cryst. Solids* **5** 365
[13] Zachariasen W H 1932 *J. Am. Chem. Soc.* **54** 3841
[14] Shevchik N J 1973 *Phys. Rev. Lett.* **31** 1245
[15] Shevchik N J, Tejeda J and Cardona M 1974 *Phys. Rev* B **9** 2627
[16] Connell G A N and Temkin R J 1974 *Phys. Rev* B **9** 5323
[17] Dixmier J, Gheorghiu A and Thèye M L 1984 *J. Phys. C: Solid State Phys.* **17** 2271
[18] Thèye M L and Gheorgiu A 1985 *Phil. Mag.* **52** 325
[19] Mott N F 1969 *Phil. Mag.* **19** 835
[20] Ziman J 1968 *J. Phys. C: Solid State Phys.* **1** 1532
Ziman J 1969 *J. Phys. C: Solid State Phys.* **2** 1230, 1704
[21] Hullinger F and Mooser E 1965 *Progress in Solid State Chemistry* ed. H Reiss (Oxford: Pergamon) p 230
[22] Shunin Yu N and Shvarts K K 1986 *Phys. Status Solidi* B **135** 15
[23] Davis E A and Mott N F 1970 *Phil. Mag.* **22** 903

[24] Mott N F 1975 *Nature* **257** 15
[25] Cohen M H, Fritzsche H and Ovshinsky S R 1969 *Phys. Rev. Lett.* **22** 1065
[26] Stuke J and Zimmerer G 1972 *Phys. Status Solidi* **49** 513
[27] Connell G A N and Paul W 1972 *J. Non-Cryst. Solids* **8–10** 215
[28] Gheorgiu A and Thèye M L 1981 *Phil. Mag* **44** 285
[29] Sénémaud C, Belin E, Gheorgiu A and Thèye M L 1985 *Solid State Commun.* **55** 947
[30] Sénémaud C, Belin E, Gheorgiu A and Thèye M L 1985 *J. Non-Cryst. Solids* **77–8** 1289
[31] Thèye M L, Gheorgiu A, Driss-Khodja K and Boccara C 1985 *J. Non-Cryst. Solids* **77–8** 1293
[32] Clerjaud B 1985 *J. Phys. C: Solid State Phys.* **18** 3615
[33] Bates C A and Stevens K W H 1986 *Rep. Prog. Phys.* **49** 783
[34] Bourgoin J C, von Bardeleben H J and Stiévenard D 1988 *J. Appl. Phys.* **64** R65
[35] Fletchter R C, Yager W A, Pearson G L, Holden A N, Read W T and Merritt F R 1954 *Phys. Rev.* **94** 1392
[36] Kaufmann U, Schneider J and Raüber A 1976 *Appl. Phys. Lett.* **29** 312
[37] Wagner R J, Krebs J J and Stauss G H 1980 *Solid State Commun.* **36** 15
[38] Elliott K, Chen R T, Greenbaum S G and Wagner R J 1984 *Appl. Phys. Lett.* **44** 907
Elliott K P, Chen R T, Greenbaum S G and Wagner R J 1984 *Proc. 3rd Conf. Insulating III–V Compounds* ed. D C Look and J S Blakemore (Shiva)
[39] Kaufmann U, Windscheif J, Baeumler M, Schneider J and Köhl F 1984 *Proc. 3rd Conf. Insulating III–V Compounds* ed. D C Look and J S Blakemore (Shiva) p 246
[40] Goswami N K, Newman R C and Whitehouse J E 1981 *Solid State Commun.* **40** 473
[41] Goltzene A, Meyer B and Schwab C 1983 *Rev. Phys. Appl.* **18** 703
Goltzene A, Meyer B and Schwab C 1984 *Proc. 3rd Conf. Insulating III–V Compounds* ed. D C Look and J S Blakemore (Shiva) p 291
Goltzene A, Meyer B and Schwab C 1984 *Phys. Status Solidi* b **123** K125
[42] Weber E R, Kaufmann U, Windscheif J, Schneider J and Wosinski T 1982 *J. Appl. Phys.* **53** 6140
Weber E R 1984 *Proc. 3rd Conf. Insulating III–V Compounds* ed. D C Look and J S Blakemore (Shiva) p 296
[43] Greenbaum S G, Treacy D J, Shanabrook B V, Comas J and Bishop S G 1984 *J. Non-Cryst. Solids* **66** 133
[44] Hoheisel B, Stuke J, Stutzmann M and Beyer W 1984 *Proc, 17th Conf. Physics of Semiconductors* ed. J D Chadi and W A Harrison (Berlin: Springer)
[45] Von Bardeleben H J, Germain P, Squelard S, Gheorgiu A and Thèye M L 1985 *J. Non-Cryst. Solids* **77–8** 1297
[46] Mauger A, von Bardeleben H J, Bourgoin J C and Lannoo M 1987 *Phys. Rev.* B **36** 5982
[47] Pauling L 1967 *The Chemical Bond* (Ithaca, New York: Cornell University Press)
[48] Michel A and Bénard J 1964 *Chimie Minérale* (Paris: Masson)
[49] Mulliken R S 1933 *J. Chem. Phys.* **1** 492
[50] Griffith J S 1964 *The Theory of Transition Metal Ions* 2nd edn (Cambridge: CUP)
[51] Van Vleck J H 1935 *J. Chem. Phys.* **3** 803
[52] Schonland D S 1971 *La Symétrie Moléculaire* (Paris: Gauthier Villars)
[53] Braunstein R 1959 *J. Phys. Chem. Solids* **8** 280
Ehrenreich H 1960 *Phys. Rev.* **15** 1951
[54] Fidone I and Stevens K W H 1959 **73** 116
[55] Goudsmit S 1931 *Phys. Rev.* **37** 663
[56] Trees R E 1953 *Phys. Rev.* **92** 308
[57] La Structure hyperfine des noyaux et des molécules, Col. Intern. CNRS Paris Juin 1966; Editions du CNRS Paris (1953) p 95
[58] Morehouse R L, Christiansen J J and Gordy W 1966 *J. Chem. Phys.* **45** 1747
[59] *Landolt–Börnstein, Zahlenwerte und Funktionen* 1952 6th edn vol I/5 p 20 (Berlin: Springer)
[60] Morton J R and Preston K F 1978 *J. Mag. Res.* **30** 577
[61] Abragam A 1961 *Les Principes du Magnétisme Nucléaire* (Saclay: INSTN)
[62] Wertz J E and Bolton J R 1972 *Electron Spin Resonance* (New York: McGraw-Hill)
[63] Kaufmann U and Schneider J 1980 *Festkörperprobleme (Advances in Solid State Physics)* vol 20 ed. (Wiesbaden: Vieweg) p 87
[64] Baeumler M, Kaufmann U and Winscheif J 1985 *Microscopic Identification of Electronic Defects in Semiconductors, San Fransisco, April 1985* (Materials Research Society Symposia Proceedings) ed. N M Johnson, S G Bishop and G D Watkins (Pittsburg: Materials Research Society) p 201
[65] Biegelsen D K and Stutzmann M 1986 *Phys. Rev.* B **33** 3006